University of Sistan and Baluchestan

Challenges in Nano and Micro Scale Science and Technology

Online ISSN: 2821 - 000X

Impact of Plasma-Coated SnO_2 Nanostructures on TiO_2 Surface for Enhanced Stability and Performance of Perovskite Solar Cells

Zeynab Kiamehr

Department of Physics, Tafresh University, Tafresh, Iran. Email: z.kiamehr@tafreshu.ac.ir

Article Info

Article type:
Research Article

Keywords:
Plasma-assisted interface engineering,
SnO_2 interfacial layer,
Electron transport layer modification,
Charge extraction and recombination suppression,
Perovskite solar cells

ABSTRACT

In this study, hydrothermally synthesized SnO_2 nanostructures deposited via a plasma-assisted process were employed as an interfacial modification layer in perovskite solar cells with an FTO/TiO_2/SnO_2/$CH_3NH_3PbI_3$/Au architecture. This low-temperature interface engineering approach enables precise modification of the TiO_2/perovskite interface without altering the bulk properties of the absorber layer. Structural and spectroscopic analyses confirm the formation of a high-purity SnO_2 phase suitable for electron transport applications. The plasma-assisted deposition facilitates the formation of a thin, uniform, and well-adhered SnO_2 interlayer under temperature conditions compatible with perovskite materials. As a result, the modified devices exhibit enhanced charge transport and extraction along with suppressed interfacial recombination. The optimized device delivers a power conversion efficiency of 20.7%, with an open-circuit voltage (V_{oc}) of 1.09 V, a short-circuit current density (J_{sc}) of 21.3 mA cm^{-2}, and a fill factor (FF) of 89%, compared to a reference TiO_2-based device with a PCE of 17.8%. These results demonstrate that plasma-assisted deposition of SnO_2 nanostructures provides a practical and scalable strategy for improving interfacial charge transport and photovoltaic performance in perovskite solar cells fabricated under ambient conditions.

INTRODUCTION

In recent years, perovskite solar cells (PSCs) have emerged as one of the most promising third-generation photovoltaic technologies, attracting extensive attention due to their remarkable rise in power conversion efficiency since 2014 [1–3]. This rapid progress has positioned PSCs as the fastest-advancing nanostructured solar cell technology to date [4]. Their appeal stems from low material costs, solution-processable fabrication routes, tunable bandgap via halide composition, and strong optical absorption, which enables efficient light harvesting with ultrathin absorber layers [5,6]. In addition, the ambipolar charge transport characteristics of perovskite materials allow efficient carrier extraction and even reasonable device performance in simplified architectures without a hole transport layer [7]. Despite these advantages, device performance and operational stability in PSCs are strongly influenced by interfacial properties, particularly at the junctions between the perovskite absorber and charge transport layers. Imperfect interfacial contact, surface defects, and energy level mismatches can hinder charge extraction and promote non-radiative recombination, ultimately limiting efficiency and long-term reliability [8]. Moreover, the polycrystalline nature of solution-processed perovskite films inevitably introduces grain boundaries and surface trap states, which serve as pathways for degradation under environmental stressors such as moisture, oxygen, heat, and illumination [9–11]. As a result, interface engineering has become a central strategy to mitigate recombination losses, improve charge transport, and enhance device stability.

In conventional n-i-p structured PSCs, compact TiO_2 is widely employed as the electron transport layer; however, its intrinsic surface defects, oxygen vacancies, and photocatalytic activity can induce interfacial recombination and accelerate perovskite degradation. To overcome these limitations, extensive efforts have been devoted to modifying TiO_2 surfaces using interfacial layers or alternative wide-bandgap materials [4,12]. Among these, SnO_2 has gained considerable attention due to its higher electron mobility, favorable conduction band alignment with perovskite absorbers, reduced photocatalytic activity, and compatibility with low-temperature processing. Previous studies have demonstrated that SnO_2-based layers can effectively passivate interfacial defects and grain boundaries, resulting in improved open-circuit voltage, short-circuit current density, and overall power conversion efficiency

How to Cite this paper: Kiamehr Z. Impact of Plasma-Coated SnO_2 Nanostructures on TiO_2 Surface for Enhanced Stability and Performance of Perovskite Solar Cells. *Challenges in Nano and Micro Scale Science and Technology*. 2025; 13(1): 50-54. DOI: 10.22111/cnmst.2026.54667.1281

Publisher: University of Sistan and Baluchestan.

DOI: 10.22111/cnmst.2026.54667.1281

[13]. For instance, Jiang et al. achieved efficiencies exceeding 21% along with enhanced moisture stability using SnO_2 interface modification [14], while Correa-Baena et al. reported superior photostability in SnO_2-based PSCs compared to TiO_2-based devices [15]. Further studies by Kim et al. and Wang et al. confirmed that nanostructured SnO_2 layers can suppress ion migration and prolong operational lifetime [16,17].

Although the beneficial role of SnO_2 in PSCs is well established, most reported approaches rely on solution-based deposition or high-temperature processing, which may suffer from limited thickness control, weak interfacial adhesion, or thermal incompatibility with perovskite materials. In this work, we report a low-temperature interface engineering strategy based on the plasma-assisted deposition of hydrothermally synthesized SnO_2 nanostructures onto TiO_2 electron transport layers. Unlike conventional approaches that replace TiO_2 entirely or require high-temperature SnO_2 processing, the present method selectively modifies the TiO_2/SnO_2 interface, enabling improved energy level alignment, enhanced electron extraction, and reduced interfacial recombination without imposing thermal or chemical stress on the perovskite absorber. The combination of controlled hydrothermal synthesis and plasma deposition allows the formation of a thin, uniform, and strongly adherent SnO_2 interfacial layer under ambient-compatible conditions, offering a scalable route to simultaneously enhance performance and stability in simplified perovskite solar cell architectures. To validate this approach, the impact of the SnO_2 interlayer on charge transport kinetics, interfacial recombination, and long-term device stability is systematically investigated through current density-voltage (J–V) characteristics, electroluminescence (EL) spectroscopy, and morphological analyses.

Experimental Section

All chemicals were used as received without further purification. Tin precursor $SnCl_4 \cdot 5H_2O$, polyvinylpyrrolidone (PVP), sodium hydroxide (NaOH), and solvents were purchased from Merck (Germany). Hydrothermally synthesized SnO_2 nanostructures were prepared by dissolving 0.351 g of $SnCl_4 \cdot 5H_2O$ in 40 mL of deionized water under magnetic stirring at 600 rpm for 30 min at room temperature to obtain a clear solution. Subsequently, 0.1 g of PVP was added as a stabilizing agent, and the solution was stirred for an additional 15 min. A 1 M NaOH solution was then added dropwise at a controlled rate of approximately one drop per second until the pH reached 10.0. After further stirring for 20 min, the resulting solution was transferred into a 50 mL Teflon-lined stainless-steel autoclave and maintained at 170 °C for 10 h to complete the hydrothermal reaction. Upon natural cooling to room temperature, the white precipitate was collected by centrifugation at 6000 rpm for 10 min, washed three times with deionized water and twice with ethanol to remove residual ions, and finally dried at 70 °C for 12 h to obtain SnO_2 nanostructured powder suitable for preparing a stable suspension.

Fluorine-doped tin oxide (FTO) glass substrates were sequentially ultrasonicated in detergent solution, deionized water, acetone, and ethanol, followed by drying under a nitrogen stream. A compact TiO_2 layer was then deposited onto the cleaned FTO substrates by RF magnetron sputtering to serve as the initial electron transport layer. The TiO_2 film thickness was controlled to approximately 40 nm and monitored in situ using a calibrated quartz crystal microbalance. After deposition, the TiO_2-coated substrates were annealed at 450 °C for 30 min in air to improve film crystallinity, density, and electronic properties before further interfacial modification.

To modify the TiO_2 surface and enhance interfacial charge transport, a SnO_2 nanostructured layer was deposited using a plasma-assisted technique, as described in Ref. [18]. In this process, a suspension containing the hydrothermally synthesized SnO_2 nanostructures was introduced into the plasma discharge region via a pneumatic nebulizer. Under an alternating electric field and controlled argon gas flow, a thin, uniform, and strongly adherent SnO_2 coating was formed on the TiO_2 surface. The plasma deposition was carried out at low temperature, ensuring the substrate remained sufficiently cool to avoid thermal damage and maintaining compatibility with subsequent perovskite layer deposition.

After forming the TiO_2/SnO_2 electron-transport structure, the perovskite absorber layer ($CH_3NH_3PbI_3$) was deposited by solution-processing. The crystallization of the perovskite film was conducted under controlled conditions to achieve a dense morphology with full surface coverage and minimal pinholes. Finally, a gold (Au) back electrode was deposited onto the perovskite layer by thermal evaporation to complete the device fabrication. The resulting perovskite solar cell architecture was $FTO/TiO_2/SnO_2/CH_3NH_3PbI_3/Au$, in which the plasma-deposited SnO_2 interfacial layer plays a crucial role in facilitating electron extraction, reducing interfacial losses, and enhancing overall device performance and stability.

The finalized device architecture and its corresponding cross-sectional morphology are summarized in Table 1 and illustrated in Figure 1. The schematic representation in Figure 1a depicts the vertical stacking sequence of the $FTO/TiO_2/SnO_2/CH_3NH_3PbI_3/Au$ device, while Table 1 provides the associated layer thicknesses and fabrication techniques. The cross-sectional SEM image shown in Figure 1b confirms the successful realization of this designed architecture, revealing well-defined and continuous interfaces between the FTO substrate, the compact TiO_2 layer, the plasma-deposited SnO_2 interlayer, and the perovskite absorber. The perovskite layer exhibits a dense morphology with a thickness of approximately 400–500 nm, in good agreement with the nominal values listed in Table 1, ensuring full coverage and effective contact with the gold back electrode. The close correspondence between the schematic design, tabulated parameters, and the SEM cross-section confirms the structural integrity and reproducibility of the fabrication process.

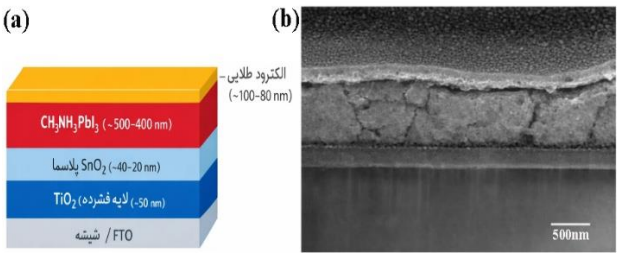

Fig. 1. Schematic illustration of the HTL-free perovskite solar cell structure and (b) cross-sectional SEM image of the fabricated device

Table 1
Layer-by-layer description of the fabricated perovskite solar cell, summarizing the deposition methods, thickness ranges, and functional roles of each layer in the FTO/TiO2/SnO2/CH3NH3PbI3/Au architecture

Layer	Deposition method	Thickness (nm)	Function
FTO	Commercial substrate	~500	Transparent electrode
TiO_2	RF magnetron sputtering	~30-50	Electron transport layer
SnO_2	Plasma coating	~20-40	Interface modification
$CH_3NH_3PbI_3$	Solution process	~400-500	Absorber layer
Au	Thermal evaporation	~80-100	Back electrode

RESULTS AND DISCUSSION

Characterization of Surface Properties

The crystal structure of SnO_2 nanostructures was investigated using X-ray diffraction (XRD) pattern (Fig. 2). As observed in the XRD pattern, distinct diffraction peaks appeared at 2θ angles of about 26.6°, 33.9°, 37.9°, 51.8°, 54.7°, 57.9°, 61.9° and 65.9°, which are attributed to the crystal planes (110), (101), (200), (211), (220), (002), (310) and (301), respectively. The XRD results confirm the successful formation of SnO_2 nanostructures with a well-defined crystal structure and are suitable for use as a modifier layer in PSCs. The absence of additional peaks or impurities indicates the appropriate phase purity of the synthesized nanostructures [19]. Also, the relatively broadened peaks indicate nanometer-sized crystals, consistent with the synthesis of nanostructured SnO_2. The high intensity of the (110) peak compared to other peaks indicates that preferential crystal growth is dominant in this plane, which is generally considered favorable for electron transport in oxide-based electron-selective layers.

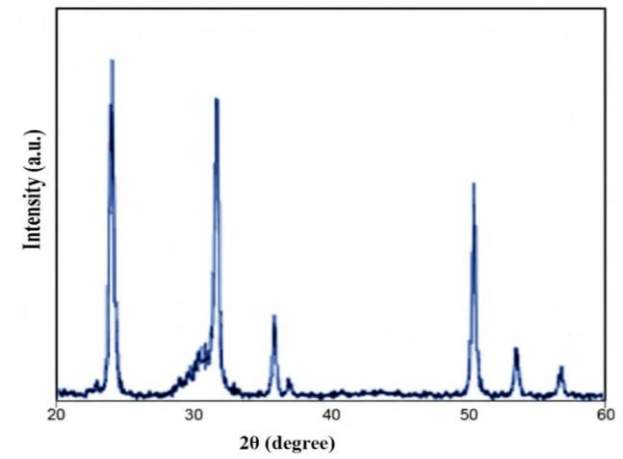

Fig. 2. X-ray diffraction pattern of hydrothermally synthesized SnO_2 nanostructures used for plasma-assisted coating on TiO_2.

Based on the FTIR pattern of SnO_2, the observed vibrational features well confirm the formation of tin oxide and the surface nature of the nanostructures (Fig. 3). The broad absorption band in the region of about 3400–3300 cm^{-1} is attributed to the stretching vibration of –OH groups, which is caused by adsorbed water molecules or surface hydroxyls on the SnO_2 nanostructures; the presence of these groups is common in nanoscale materials and is related to the high surface energy of the particles. The weaker peak in the range of 1630–1650 cm^{-1} is related to the bending vibration of adsorbed water molecules (H–O–H bending), which also confirms the presence of physical moisture or surface hydroxyl groups. The bands observed in the region of 1000–1400 cm^{-1} can be attributed to the Sn–O–Sn vibrations or the weak surface-related vibrations commonly observed in metal oxide nanostructures, although their intensity is relatively low [20]. The most important feature of the spectrum is the strong and distinct absorption in the region of 500–650 cm^{-1}, which is related to the stretching vibration of the Sn–O bond and is the main indicator of the formation of the SnO_2 phase. The presence of this strong band in the low-frequency region indicates the successful formation of the SnO_2 oxide network.

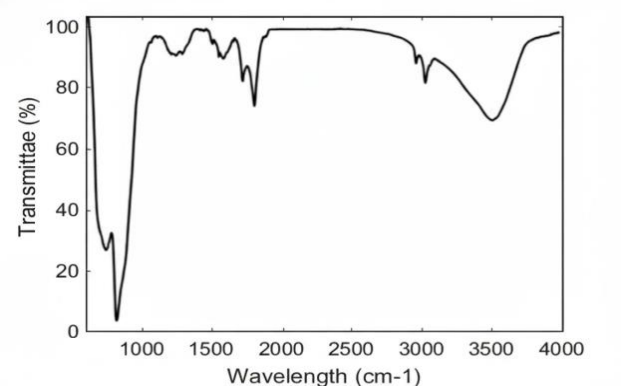

Fig. 3. The FTIR analysis of the SnO_2 nanostructures coated on TiO_2 by the plasma method

Voltage-Current Density Characteristic

The current density–voltage (J–V) characteristics reveal a clear performance difference between devices fabricated with and without the SnO_2 interlayer (Fig. 4). At zero applied voltage, the short-circuit current density of the TiO_2/SnO_2-based device is slightly higher than that of the pristine TiO_2 device, suggesting more efficient charge extraction and reduced interfacial losses at the ETL/perovskite interface.

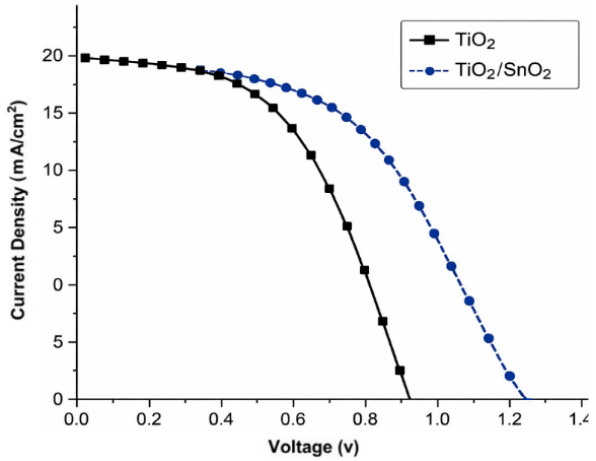

Fig. 4. Current-voltage spectrum of fabricated PSCs

A more pronounced difference is observed in the open-circuit voltage, where the TiO_2/SnO_2 structure exhibits a noticeably higher V_{oc}. This enhancement is commonly associated with suppressed non-radiative recombination and improved interfacial energetics upon introducing the SnO_2 layer. In addition, the smoother current decay and the shift of the knee region toward higher voltages in the TiO_2/SnO_2 device indicate a reduction in series resistance and a corresponding improvement in the fill factor. In contrast, the steeper current drop observed for the pure TiO_2 device implies higher recombination losses and less efficient charge transport, which is consistent with previous reports on TiO_2-based electron transport layers [21–23].

Luminescence Characteristic

Figure 5 presents the electroluminescence (EL) spectra of the perovskite solar cells before and after plasma-assisted coating of SnO_2 nanostructures. For both devices, the main emission peak appears in the wavelength range of approximately 560–580 nm, indicating that the bandgap and intrinsic optical properties of the perovskite absorber remain unchanged after introducing the SnO_2 layer. This observation confirms that the SnO_2 coating primarily acts as an interfacial modification layer rather than altering the bulk properties of the perovskite film. Notably, the EL emission intensity of the TiO_2/SnO_2-based device is significantly lower than that of the TiO_2 reference sample. Such a reduction in EL intensity is commonly associated with more efficient charge extraction at the electron transport layer/perovskite interface, whereby injected electrons are transferred into the ETL before undergoing radiative recombination with holes in the perovskite layer. Consequently, carrier accumulation under forward bias is suppressed, leading to diminished EL emission despite improved photovoltaic performance.

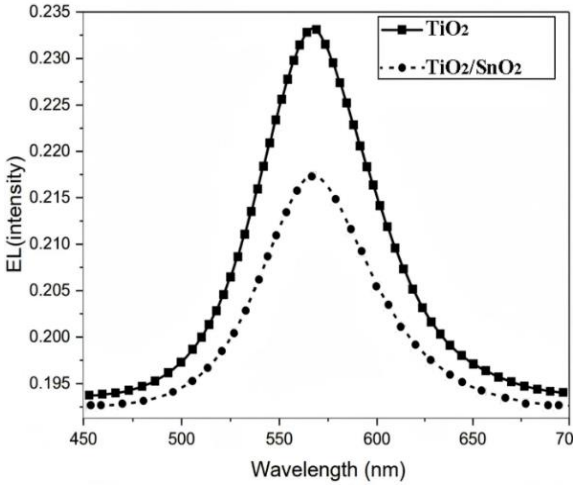

Fig. 5. Electroluminescence spectrum of fabricated diodes

This behavior suggests that the plasma-deposited SnO_2 nanostructures facilitate electron transport and collection at the interface. Moreover, the SnO_2 interlayer is expected to passivate surface defects and trap states at the TiO_2/perovskite interface, which otherwise act as recombination centers in the unmodified device and contribute to higher EL intensity. The observed suppression of EL emission in the modified sample therefore indicates an effective inhibition of these recombination pathways [24-28]. In addition, the higher electron mobility of SnO_2 compared to TiO_2 further promotes efficient electron transport and reduces charge accumulation at the interface, which is consistent with reduced radiative recombination under electrical injection conditions.

CONCLUSION

The interfacial modification of TiO_2 electron transport layers using hydrothermally synthesized SnO_2 nanostructures deposited via a plasma-assisted process was systematically investigated as an effective route to enhance the photovoltaic performance of perovskite solar cells. Structural analyses confirmed the formation of a pure and crystalline SnO_2 phase with characteristics suitable for interfacial electron transport. The plasma-assisted technique enabled the formation of a thin, uniform, and strongly adherent SnO_2 interlayer at low temperature, ensuring compatibility with solution-processed perovskite absorbers and offering a controllable alternative to conventional deposition methods.

Photovoltaic measurements revealed a significant improvement in device parameters upon introducing the SnO_2 interlayer. The TiO_2/SnO_2-based devices exhibited higher open-circuit voltage, increased short-circuit current density, and an improved fill factor compared to reference TiO_2-only cells, resulting in a marked enhancement of power conversion efficiency. These improvements are attributed to more favorable interfacial energetics, reduced interfacial resistance, and suppressed trap-assisted recombination at the TiO_2/perovskite interface.

Electroluminescence measurements further supported this interpretation, showing a reduced emission intensity for the SnO_2-modified devices while maintaining an unchanged emission peak position, indicative of efficient charge extraction and reduced carrier accumulation under forward bias. Therefore, this work demonstrates that plasma-assisted deposition of SnO_2 nanostructures represents a practical and effective interface engineering strategy to improve charge transport and reduce recombination losses in TiO_2-based perovskite solar cells. The approach provides a scalable, low-temperature pathway for enhancing device performance through precise interfacial modification, without altering the bulk properties of the perovskite absorber.

REFERENCES

[1] O'Regan B, Grätzel M. A low-cost, high-efficiency solar cell based on dye-sensitized colloidal TiO2 films. Nature. 1991;353:737–740.

[2] Bach U, Lupo D, Comte P, Moser JE, Weissörtel F, Salbeck J, et al. Solid-state dye-sensitized mesoporous TiO2 solar cells with high photon-to-electron conversion efficiencies. Nature. 1998;395:583–585.

[3] Chen F. Introduction to plasma physics and controlled fusion. 1984.

[4] Das S, Neogi S, Mukherjee M. Effect of temperature and deposition rate on the surface morphology of thin Al metal films on glass substrate: application in solar cell. J Phys Conf Ser. 2020;12:012019.

[5] Yahya M, Fadavieslam M. The effects of argon plasma treatment on ITO properties and the performance of OLED devices. Opt Mater. 2021;120:111400.

[6] Sree Harsha KS. Principles of vapor deposition of thin films. 2006.

[7] Kiamehr Z. Improving the performance of polyvinyl alcohol membrane by deposition of graphene oxide nanostructures using non-thermal plasma. Challenges Nano Micro Scale Sci Technol. 2025;11:18–23.

[8] Yuji T, Akatsuka H, Mungkung N, Park BW, Sung YM. Surface treatment of TiO2 films for dye-sensitized solar cells using atmospheric-pressure non-equilibrium DC pulse discharge plasma jet. 2009;83:124–127.

[9] Jin H, Kim J, Hong B. Effect of hydrogen plasma treatment on nano-structured TiO2 films for enhanced performance of dye-sensitized solar cell. Appl Surf Sci. 2013;274:171–175.

[10] Karabay I, Yüksel S, Ongül F, Öztürk S, Aslı M. Structural and optical characterization of TiO2 thin films prepared by sol–gel process. 2012;121:265–267.

[11] Chen F. Introduction to plasma physics and controlled fusion. 1984.

[12] Sree Harsha KS. Principles of vapor deposition of thin films. 2006.

[13] Ermolaeva S, et al. Non-thermal argon plasma is bactericidal for the intracellular bacterial pathogen Chlamydia trachomatis. J Med Microbiol. 2012;61:793–799.

[14] Jiang H, et al. Synergistic strategy of anion and cation at the SnO2/perovskite interface constructing efficient and stable solar cells. Wiley Online Library. 2025.

[15] Correa Baena J. Doped-tin oxide aerogels in dye-sensitized solar cells. 2014. Available from: digitalcommons.lib.uconn.edu

[16] Kim S. Effects of potassium treatment on SnO2 electron transport layers for improvements of perovskite solar cells. Energy. 2022.

[17] Wang J, et al. Insights into fullerene passivation of SnO2 electron transport layers in perovskite solar cells. 2019.

[18] Kiamehr Z. Improving the performance of polyvinyl alcohol membrane by deposition of graphene oxide nanostructures using non-thermal plasma. Challenges Nano Micro Scale Sci Technol. 2025;11:18–23.

[19] Jha R. Solar cell technology and application. New York: Taylor and Francis Group, LLC; 2010.

[20] Tubtimtae A, Lee M, Wang G. Ag2Se quantum-dot sensitized solar cells for full solar spectrum light harvesting. J Power Sources. 2011;196:6603–6608.

[21] Green MA. The path to 25% silicon solar cell efficiency: history of silicon cell evolution. Prog Photovolt Res Appl. 2009;17:183–189.

[22] Nazeeruddin MK, Zakeeruddin SM, Lagref J, Liska P, Comte P, Barolo C, et al. Stepwise assembly of amphiphilic ruthenium sensitizers and their applications in dye-sensitized solar cells. Coord Chem Rev. 2004;248:1317–1328.

[23] Tubtimtae K, Wu KL, Tung H, Lee M, Wang G. Ag2S quantum dot-sensitized solar cell. Electrochem Commun. 2010;12:1158–1160.

[24] Imahori H, Hayashi S, Hayashi H, Oguro A, Eu S, Umeyama T, et al. Effects of porphyrin substituents and adsorption conditions on photovoltaic properties of porphyrin-sensitized TiO2 cells. J Phys Chem C. 2009;113:18406–18413.

[25] Chen J, Li C, Zhao DW, Lei W, Zhang Y, Cole M, et al. A quantum dot sensitized solar cell based on vertically aligned carbon nanotube templated ZnO arrays. Electrochem Commun. 2010;12:1432–1435.

[26] Tress W. Interpretation and limitations of electroluminescence measurements in perovskite solar cells. Adv Energy Mater. 2017;7:1602358.

[27] Stolterfoht M, et al. Visualization and suppression of interfacial recombination for high-efficiency large-area pin perovskite solar cells. Nat Energy. 2018;3:847.

[28] Rau U. Reciprocity relation between photovoltaic quantum efficiency and electroluminescent emission of solar cells. Phys Rev B. 2007;76:085303.